Published in final edited form as:
Circ Res. 2010 March 19; 106(5): 981–991. doi:10.1161/CIRCRESAHA.109.204891.

Transmural Dispersion of Repolarization in Failing and Non Failing Human Ventricle

Alexey V. Glukhov, PhD, **Vadim V. Fedorov, PhD**, **Qing Lou, BS**, **Vinod K. Ravikumar**, **Paul W. Kalish**, **Richard B. Schuessler, PhD**, **Nader Moazami, MD**, and **Igor R. Efimov, PhD**
From the Department of Biomedical Engineering (A.V.G., V.V.F., Q.L., V.K.R., P.W.K., I.R.E.) and Surgery (R.B.S., N.M.), Washington University in St. Louis, MO, USA

Abstract

Rationale—Transmural dispersion of repolarization has been shown to play a role in the genesis of ventricular tachycardia and fibrillation in different animal models of heart failure (HF). Heterogeneous changes of repolarization within the midmyocardial population of ventricular cells have been considered an important contributor to the HF phenotype. However, there is limited electrophysiological data from the human heart.

Objective—To study electrophysiological remodeling of transmural repolarization in the failing and non-failing human hearts.

Methods and Results—We optically mapped the action potential duration (APD) in the coronary-perfused scar-free posterior-lateral left ventricular free wall wedge preparations from failing (n=5) and non-failing (n=5) human hearts. During slow pacing (S1S1= 2,000ms), in the non-failing hearts we observed significant transmural APD gradient: subepicardial, midmyocardial, and subendocardial APD80 were 383±21ms, 455±20ms, and 494±22ms, respectively. In 60% of non-failing hearts (3 of 5), we found midmyocardial islands of cells that presented a distinctly long APD (537±40ms) and a steep local APD gradient (27±7ms/mm) compared with the neighboring myocardium. HF resulted in prolongation of APD80: 477±22ms, 495±29ms, and 506±35ms for the subepi-, mid- and subendocardium, respectively, while reducing transmural APD80 difference from 111±13ms to 29 ±6ms (p<0.005) and presence of any prominent local APD gradient. In HF, immunostaining revealed a significant reduction of Cx43 expression on the subepicardium.

Conclusions—We present for the first time direct experimental evidence of a transmural APD gradient in the human heart. HF results in the heterogeneous prolongation of APD, which significantly reduces the transmural and local APD gradients.

Keywords

Heart failure; repolarization; transmural gradient; optical mapping; connexin43

INTRODUCTION

Heart failure (HF) claims over 200,000 lives annually in the US alone.[1, 2] Approximately a half of these deaths are sudden and presumably due to ventricular tachyarrhythmias.

Corresponding author: Igor R. Efimov, Department of Biomedical Engineering, Washington University in St. Louis, MO 63130. Tel: 1-314-935-8612; Fax: 1-314-935-8377; igor@wustl.edu.

Previously reported as preliminary results in abstract form (Circulation 2008; 118: S_397).

Disclosure
None.

Pathophysiological remodeling of cardiac function occurs at multiple levels and includes the alterations in a host of ion channels, Ca^{2+}-handling proteins, and proteins mediating cell-cell coupling, predisposing to arrhythmias and sudden death.[3] Numerous animal models have shown the importance of such electrophysiological (EP) remodeling in the mechanisms of HF-related arrhythmogenesis.[4]

Prolongation of the repolarization is a hallmark of cells and tissues isolated from failing hearts independent of the cause, which has been observed in isolated myocytes[5] and intact ventricular preparations.[4, 6] This fundamental change in myocyte biology underlies QT-interval prolongation of the surface electrocardiogram in patients with HF. The action potential prolongation is heterogeneous, resulting in exaggeration of the physiological heterogeneity of electrical properties in the failing heart.[1, 4] These cellular EP changes were linked to downregulation of potassium currents (I_{to}, I_{Kr}, I_{Ks}, and I_{K1}), an increase in late Na current (I_{Na}) density, as well as significant changes in intracellular calcium handling proteins.[1–3] However, despite these studies a direct mechanistic link between repolarization changes observed in isolated myocytes or on the body surface and arrhythmia genesis remained lacking, largely because of technical difficulties in assessing the functional expression of spatiotemporal repolarization changes at the intact heart level.

Transmural dispersion of repolarization has been suggested to play an important role in the genesis of polymorphic ventricular tachycardia in different animal models of HF.[4, 7, 8] In the normal human ventricular myocardium, at least three different populations of cells — subepicardial, subendocardial, and midmyocardial (M-cells) — are selected based on their different native EP properties and different responses to drugs.[8–12] Studies in isolated tissues and myocytes showed that HF associated action potential prolongation is heterogeneous across the left ventricle (LV) wall, affecting different transmural layers in different ways[13] and thereby increasing the effective transmural repolarization gradient.[4, 14, 15] At the same time, Taggart et al. [16] have been unable to detect physiologically significant transmural gradient in patients, even during pronounced bradycardia as well as during early ischemia. These discrepancies were explained by the cell injury or cell-cell uncoupling caused by cell isolation or tissue dissection, by influence of local environment of cells, or by use of anesthetic agents in the in vivo studies that suppress transmural dispersion of repolarization.[17–20] However, this study did not investigate the effect of HF on the transmural repolarization and presented a combination of patients with different etiology.[16] In view of the EP differences between different studies and limited information from the human heart, in this study we optically mapped transmural wedge preparation from failing and non-failing human hearts. We also mapped immunostaining for expression of Cx43 through the LV wall.

METHODS

A detailed Methods section is provided in the Online Supplement.

Patients groups

Failing hearts (n=5, Online Table I) with different types of cardiomyopathy were obtained during transplantation at the Barnes-Jewish Hospital, Washington University in Saint Louis, MO. For comparison, we used non-failing donor hearts (n=5, Online Table II), which were rejected for transplantation for various reasons, including age, early stage hypertrophy, atrial fibrillation, and coronary disease. Donor hearts were provided by the Mid-America Transplant Services (Saint Louis, MO). The study was approved by the Washington University Institutional Review Board.

Explanted hearts were cardioplegically arrested and cooled to 4–7°C in the operating room following crossclamping of the aorta. The arrested heart was maintained at 4–7°C to preserve tissue during 15–20 minutes delivery from the operating room to the research laboratory.

Experimental preparation

We isolated wedges of human ventricular wall as previously described in canine heart.[17,18] Briefly, after harvesting, the hearts were immediately perfused through the aorta with a cardioplegic solution (in mmol/l: NaCl 110, CaCl2 1.2, KCl 16, MgCl2 16, NaHCO3 10, 4° C). The cardioplegic perfusion washed out the blood and protected the hearts during the subsequent period of wedge isolation. We then isolated a transmural wedge from the posterior-lateral left ventricular (LV) free wall supplied by left marginal artery (Fig. 1A). The preparation was dissected several centimeters below the base of the ventricles and extended about 3 cm towards the apex (Fig. 1A, B). The thickness of the LV was not differ between non-failing and failing wedge preparations (16.6±1.4 mm vs 19.2±1.5 mm, respectively, p=0.26; see also Online Table III). Each wedge contained a section of coronary artery (diameter ≥1 mm) along its length, which was cannulated with the flexible plastic cannula custom made for these experiments. Major arterial leaks in the wedges were ligated with silk suture. The quality of perfusion was verified by injection of Methylene Blue dye (Sigma, St. Louis, MO). Poorly perfused tissue was trimmed from the wedges. The isolated tissues were mounted in a warm chamber with the dissected exposed transmural surface up, facing the optical apparatus. Wedges were perfused with oxygenated Tyrode solution composed of(in mmol/l): 128.2 NaCl, 4.7 KCl, 1.19 NaH_2PO_4, 1.05 $MgCl_2$, 1.3 $CaCl_2$, 20.0 $NaHCO_3$, and 11.1 glucose, and gassed with 95%O_2-5% CO_2; pH=7.35±0.05. We maintained 37°C and an arterial pressure of 60–70 mmHg. The preparation was fully immersedin the perfusion efflux, which assured appropriate superfusion.

Imaging system

After 20–30 minutes of washout, gradual warming after cold cardioplegia to 37°C, tissue recovery, and stabilization, the wedges were stained with 4 μM di-4-ANEPPS (Molecular Probes, Eugene, OR), a membrane potential-sensitive fluorescent dye having no known electrophysiological effects and used widely in optical mapping studies in hearts of many species.

We immobilized the wedges with 10 μM Blebbistatin (Tocris Bioscience, Ellisville, MO) which inhibits the adenosine triphosphatases (ATPases) associated with class II myosin isoforms in an actin-detached state, and thus successfully blocks cardiac contraction without any effect on electrical activity, including ECG parameters, atrial and ventricular effective refractory periods, and atrial and ventricular activation patterns in many mammalian species.[21, 22] We used microelectrode recordings to validate the effect of Blebbistatin in the human ventricle (see Online Supplement).

The wedges were paced at the endocardium by 5–10 ms pulses at 2 × diastolic current thresholds at a pacing cycle length (CL) ranging from 4,000ms to the ventricular functional refractory period. Two Ag/AgCl electrodes were immersed into the superfusion solution, one at the epicardial and the other at the endocardial side, to document the transmural pseudo-ECG (Fig. 1C).

An optical mapping system[23] with a 100×100 pixels resolution MiCAM Ultima-L CMOS camera (SciMedia, USA Ltd., CA) collected the fluorescent light from an area of 2–3 cm by 2–3 cm (Fig. 1B) on the cut-exposed transmural surface of the wedge. Optical action potentials (APs) were recorded from the transmural optical field of view (20×20 to 30×30 mm^2) with a spatial resolution of 200–300 μm/pixel at a rate of 1,000 frames/s (Fig. 1C). The fluorescent

signals were amplified, digitized, and visualized during experiment using specialized software (SciMedia, USA Ltd., CA)

Data processing

A custom-made Matlab-based computer program was used to analyze APs offline.[24] First, the signals were filtered using the low-pass Butterworth filter at 50 Hz. Activation maps were constructed from activation times, which were determined from the dV/dt_{max} in each channel. Finally, AP duration was calculated as time difference between the activation time (dV/dt_{max}) and 80% of repolarization (APD80)..

Local APD gradient was measured as the APD difference of neighboring pixels over the pixel length after 3 by 3 average filtering. To estimate size and area of islands of prolonged APD, we used criteria based on the local APD gradient with the threshold of 15 mm/ms. Maximum APD within local high-APD-gradient boundary line was identified and then used as a threshold for the island with prolonged repolarization. For detailed description of data analyses see Online Supplement.

Restitution protocol

The dependence of APD80 on the preceding diastolic interval (DI) was determined using the dynamic restitution protocol as described earlier.[25] Preparations were paced at a constant basic CL, which was shortened from 4,000 to 1,000 ms in steps of 500 ms, from 1,000 to 500 in step of 100 ms, and in steps of 10 ms from 400 ms until ventricular functional refractory period was reached. We observed APD alternans at short CL. In order to measure APD of both long and short APs during alternans, we repeated pacing protocol twice. The relationship between APD and DI was determined by plotting of APD80 as a function of DI as described elsewhere.[26] The steep portion of the restitution was linearly approximated for measurement of slopes. Slopes were determined by linear fitting of the steep portion of the restitution curve, which contains a 30-ms DI segments data without APD alternans.

APD alternans was quantified by computing ΔAPD for two consecutive beats. Similarly, AP amplitude alternans was quantified by computing the amplitude differences of two consecutive beats as described elsewhere.[26]

Histology and Immunofluorescence labeling

Histology experiments were performed as previously described.[27] Sections were stained with Masson's trichrome (International Medical Equipment, San Marcos, CA, USA). The examples of histological staining for subepicardial, midmyocardial, and subendocardial sections are presented on Online Figure VA. Immunolabeling was carried out as described previously.[25, 27, 28] Sections were stained with commercially available antibodies: Rabbit Cx43 (Sigma, 1:1000) and Mouse α-actinin (Sigma, 1:1600). Protein density was measured using the NIH ImageJ software as previously described.[27] For details see Online Supplement.

Statistical analysis

Values are expressed as means ± SEM. Hypothesis testing was carried out using an unpaired student t-test and chi-squared analysis with Yates correction. A value of $p<0.05$ was considered statistically significant.

RESULTS

Transmural dispersion of repolarization in human LV

Figure 2 shows maps of transmural activation and APD and representative subepicardial, midmyocardial, and subendocardial APs from two representative examples of the human non-failing (A, heart #3) and failing (B, heart #4) LV wedges. Presented data were obtained during bradycardia pacing at 30 beats/min (CL=2,000 ms). The hearts were paced from the endocardium following normal excitation sequence as was performed in earlier studies in the canine preparation.[4, 7, 17] The maps demonstrated the homogeneous activation patterns without conduction delays or blocks indicating the quality of preparation perfusion, tissue condition, and robust cell-cell coupling. Transmural activation time was in agreement with Durrer et al. [29] The average transmural conduction velocity was 41.4±10.6 cm/s (n=10) at 30 beats/min.

In non-failing human LV, we observed significant differences between APD at the subepicardium versus the subendocardium and midmyocardium (Fig. 3A), which resulted in a substantial transmural APD gradient (Fig. 3D). HF remodeling induced transmurally heterogeneous prolongation of APD, which resulted in a significantly stronger lengthening of APD at the subepicardium than at the subendocardium and midmyocardium (Figs. 3B and 3C). The average functional refractory period for fast pacing was also increased in failing ventricles (from 258±23 ms to 377±37 ms ($p<0.05$), for non-failing and failing groups respectively). Thus, HF resulted in a significant reduction of the total transmural APD gradient between the subendocardium and subepicardium (Fig. 3D). A representative example is illustrated in Figure 5A2. See also Online Figure IVB with two more examples from the other failing hearts and Online Tables II and III with all data for transmural APD distribution in non-failing and failing hearts.

We found two different patterns of transmural APD distribution. The first pattern was observed in 100% of failing hearts and in 40% of non-failing donor's hearts (2 out of 5) and was characterized by a smooth decrease in APD from the subendocardium to the subepicardium without prominent peaks and valleys or strong local gradients. However, in 60% (3 out of 5) non-failing hearts, we found islands of cells, which were localized in deep subendocardium or midmyocardium and possessed a distinctly long APD compared with the neighboring myocardium. See Online Figure III with all five examples of APD distribution in non-failing hearts. The average APD values for these islands were calculated in these three hearts and presented as a separate group (Max-APD) in Figures 3A and 3B. Examples of APD distribution in non-failing hearts are presented in Figure 2 (heart #4), Figure 5 (heart #2) and Online Figure IV (hearts #3 and #4).

To describe these islands in detail, we quantified the transmural APD distribution throughout the mapped area. We found a relatively gradual increase in APD from the subepicardium to the mid-myocardium followed by a sharp increase in APD in the subendocardium. However, the observed areas of delayed repolarization (Max-APD) did not form continuous layers, but rather formed isolated islands. Figure 4 illustrates this by showing two APD distributions in the same LV wedge preparation taken along the different transmural lines, which are perpendicular to the epi- and endocardium. The first distribution (Fig. 4B1) shows a gradual APD shortening from the subendocardium to the subepicardium without prominent peaks or sharp gradients. In contrast, the second distribution (Fig. 4B2) crosses the deep subendocardial island of delayed repolarization and contains a steep transmural APD gradient with a sharp gradient of APD in the deep subendocardial region marked by the red rectangle on Fig. 4B2. Thus, very different transmural APD distribution can be observed depending on the choice of anatomic cross section or area of subendocardium. Therefore, we conclude that characterization of heterogeneity of transmural gradient by means of APD distribution along a transmural line may be limited and requires the two dimensional mapping. This ambiguity

is especially important for microelectrode studies where the high-density 2D mapping of transmural APD is impossible.

To characterize these islands further, we established a criterion based on the local APD gradient between them and the neighboring myocardium. Red rectangle in Figure 4B2 marks the distribution of the APD through the Max-APD island. This example demonstrates a sharp transition of APD in the subendocardium characterized by the large local APD gradient (Figures 4C and 4D). We defined Max-APD islands as regions isolated from the neighbors by local APD gradient of >15 ms/mm. Figure 4D shows the vector map of APD gradient in a close-up view of the Max-APD island, and the Figure 4E shows the magnitude map of APD gradient. Figures 4E and 4E demonstrate that the Max-APD island was surrounded by the maximum of the local APD gradient (deep red color). The average size of Max-APD islands was 9.2±2.0 mm^2 (n=3). All Max-APD islands as well as local APD gradient distributions for other two non-failing human hearts are presented in Online Figure II. In all three non-failing hearts, Max-APD islands were located in the deep subendocardium as presented in Figure 4. The center of these islands was located approximately at 3.4±0.3 mm apart the endocardium (4.1 mm, 3.1 mm, and 3.1 mm for hearts #1, #4, and #5 respectively). In one non-failing heart #4, we found two islands with prolonged repolarization; one of them was located in the midmyocardium (approximately 9.1 mm apart the endocardium) and did not completely fit by the optical field of view (see Online Figure II); we did not include it in the analysis. Dimensions of Max-APD islands were 2.4±0.6 mm in depth and 4.7±2.2 mm in maximum length on average (n=3).

Progressive shortening of the pacing CL up to the functional refractory period resulted in shortening of APD and decrease of transmural APD gradient (see Fig. 3A and B). Figure 5 demonstrates the activation and the APD distribution patterns and representative subepicardial, midmyocardial, and subendocardial APs from two typical non-failing (A) and failing (B) human LV wedge preparations. Data are presented for the non-failing heart #5 and failing heart #2. Three pacing CLs from the applied restitution protocol are shown. Progressive decrease of pacing CL resulted in slowing of activation and shortening of APD throughout the wedges. Moreover, APD shortening occurred heterogeneously in the non-failing hearts and eliminated the transmural APD gradient. For example, during slow pacing at 15 bpm (Fig. 5A1) the selected non-failing wedge exhibited a significant transmural APD gradient of about 180 ms with prominent APD in midmyocardium areas. However, during fast pacing at 120 bpm (Fig. 5C1) the transmural APD gradient decreased nearly in half down to 90 ms, and the endocardial and midmyocardial APD became comparable. As described earlier, the failing heart showed reduced transmural APD gradient without a significant APD difference between the subendocardium and midmyocardium. Thus, in failing hearts, fast pacing also decreased transmural APD gradient in half (from 70 ms to 35 ms, on Fig. 5A2 and Fig. 5C2 respectively) and fully equalized the endocardial and midmyocardial APD.

Dynamic properties of transmural repolarization

It has been previously shown that the rate dependence of APD is heterogeneously distributed through the mammalian LV.[9, 10, 30] To characterize the dynamic properties of transmural repolarization, we applied the restitution protocol for all tested human hearts. As shown on Figure 5, in the non-failing hearts, progressive decrease in pacing CL resulted in heterogeneous APD shortening throughout the LV wedge preparation. In agreement with animal studies,[8–10, 17, 30] deceleration-induced prolongation of APD in the non-failing hearts was much greater in midmyocardial area than in subepicardial and subendocardial regions (Fig. 6B). Maps show spatial distributions of APD restitution slopes through the LV free wall in representative non-failing (Fig. 6A, non-heart #5) and failing (Fig. 6C, failing heart #2) human hearts. The color scales represent the value of maximal restitution slope in every single pixel. As indicated by

color scales, values of slope for non-failing heart (A) were significantly higher than for failing heart (C) and significantly exceeded the critical threshold value of one as compared to failing heart where slopes were lower than one throughout the mapped area. Plotted for different regions, the APD restitution curve for midmyocardial area (i.e. for Max-APD islands) revealed a steeper slope as compared to the subepicardium and subendocardium (Fig. 6B). In contrast, failing hearts were characterized by approximately equal restitution slopes in the midmyocardium, subepicardium, and subendocardium (Fig. 6D). The average APD restitution slopes throughout the mapped area were 1.10±0.09 (n=5) and 0.86±0.12 (n=5) for non-failing and failing hearts, respectively.

Different restitution kinetics in the Max-APD islands resulted in the presence of electrical alternans in these regions. Figure 7 shows the dynamics and anatomic locations of APD alternans (A) and AP amplitude alternans (B) in non-failing heart #5. Four panels in (A) and (B) represent transmural distribution of each type of alternans during progressive decrease of pacing CL. The black areas on maps indicate that the algorithm for APD alternans calculation could not be applied because of incomplete repolarization at this CL or low quality of optical signals. It is evident that alternans of APD started first at CL=260ms. Figure 7C shows distribution of diastolic intervals as well as corresponding APDs plotted for each pixel during pacing with CL=240ms. The separation of areas with single colors (red or green) indicates the presence of alternans at this pacing frequency. The representative examples of optical recordings from three areas labeled on maps are shown in Figure 7D. APD alternans were observed in 80% (4 out of 5) of non-failing hearts. We did not observe alternans in the non-failing heart #4. The most predominant location of APD alternans was subendocardium. The pacing CL threshold for APD alternans occurrence in non-failing hearts was 335±45 ms (n=4). In failing hearts, APD alternans were observed only in heart #3, (20% hearts, 1 out of 5) during pacing with CL=300 ms. However, in two failing hearts (#1 and #2) we could not induce APD alternans. Therefore, obtained data do not allow us to relate HF remodeling and APD alternans. Additionally, we did not observe any evidence of extrabeats and/or arrhythmias in both non-failing and failing human LV wedges. Neither during slow pacing (CL=4,000 ms) nor after termination of fast pacing of restitution protocol there were changes in resting potentials, which could be interpreted as triggered arrhythmia.

Transmural expression of connexin 43

To examine the transmural Cx43 expression in the human heart, optically mapped tissues were studied by immunohistochemistry. Figure 8A represents typical examples of Cx43/α-actinin double immunostained tissues from non-failing and failing hearts taken from epicardial, midmyocardial, and endocardial locations. The epicardial Cx43 density in both non-failing and failing hearts was found to be significantly decreased compared with the midmyocardial and endocardial expression (Fig. 8B). Heart failure remodeling resulted in a significant decrease of relative transmural expression of Cx43 on the subepicardium. Midmyocardial and subendocardial Cx43 tended to downregulate as well in failing hearts, but the difference with non-failing hearts did not reach statistical significance.

DISCUSSION

Our study shows that LV remodeling in the human failing heart results in (1) an increase of APD and refractory period, (2) reduction of the maximum slope of APD restitution curve, (3) reduction of local and global transmural APD gradient, (4) occurrence of APD and AP amplitude alternans, and (5) downregulation of subendocardial Cx43 expression.

Heart failure remodeling

QT-interval prolongation is a well-recognized hallmark of human and experimental HF.[1–5] In this study, in failing hearts we also observed prolongation of functional refractory period as well as transmural APD through the LV (Figs. 2 and 3). When compared to non-failing hearts, end-stage failing hearts demonstrated transmurally heterogeneous prolongation of APD, which was evident in a significantly higher lengthening of APD at the subepicardium as compared to the subendocardium and midmyocardium (Fig. 3). As a result, the total transmural APD gradient between the subendocardium and subepicardium was significantly decreased during HF (Fig. 3D) as also shown in examples in Figures 2A and 5A2 (see also Online Figure IVB). Interestingly, reduction of transmural APD gradient in LV is contrary to animal models data demonstrated an enhanced transmural heterogeneity in canine failing hearts.[4] It should be noted that all animal data were presented from the 4–6 weeks rapid pacing model of HF. In contrast, in our study we used human hearts from patients with the end-stage HF, which was progressing over long time (see Online Table 1). It may appear that our findings contradict general consensus on overall increase in dispersion of repolarization in failing hearts. However, we believe it is not so. It is known that both structural and ionic remodeling contribute to increase in dispersion of repolarization. In our study we excluded structural remodeling as a factor by selecting wedges without prominent scarring and fibrosis. In addition, we focused only on mid-wall transmural myocardium, while there is a possibility of apical-basal APD gradient, which has been demonstrated in several species.[31] Finally, only one transmural section was mapped in each human heart and therefore we cannot exclude the possibility that other regions might have APD heterogeneity.

Our results are in agreement with observation of Taggart at al. [16] from 21 patients (44–84 years old) with different anamnesis. In that study, the physiologically significant transmural gradient within the ventricular wall was absent even during both pronounced bradycardia and early ischemia.[16] These changes between early and end-stage HF are likely due to remodeling in ion channel and calcium handling protein expression.[2, 3] In the current study, we have not investigated these changes, and would abstain from unsubstantiated speculations. However, we are in the process of mapping transmural differences in mRNA and protein expression, which will be reported in a follow-up study.

M-cells

We provide for the first time experimental evidence in support of existence in the non-failing human heart of a distinct population of subendocardial cells with significantly delayed repolarization as compared to the neighboring myocardium (Fig. 4). These isolated islands are characterized by steep local APD gradient (Fig. 4) and different restitution properties (Figs. 6). The observed islands of cells with significantly prolonged repolarization appeared to be similar to a midmyocardial population, known as M-cells, which was observed in several animal models.[4, 7, 12, 17] However, in contrast to some reports from animal models, we did not observe contiguous layers of cells in the midmyocardium or deep subepicardium which were referred to the M-cell population.[13, 30] In contrast, we found the isolated islands of delayed repolarization, in agreement with canine data reported by Akar et al.[7] Interestingly, in contrast to non-failing human hearts, failing hearts demonstrated a relatively flat APD distribution throughout the LV wall without prominent peaks (Figs. 5), which could be referred to as M-cell islands.

The original definition of M-cells, a distinctive class of midmyocardial cells having exceedingly long APD, when activated at long CLs characteristically different and separated from the subepicardial and subendocardial myocytes[9, 30], was based on observations with microelectrode recordings at selected sites. Although M-cells were defined, the criteria for separating from other cell types have been less clear. In addition, the differences in the APDs

between the M-cells and surrounding subendocardium were much smaller in intact canine ventricular wall compared with isolated cells or tissues[18, 32] as also observed in our study in humans (Figs. 4 and 5). Yan et al.[33] reported that the difference between the above mean APDs (15 ms) was actually smaller than their standard deviations (25 and 21 ms). Such a relatively small difference in APD may not be easily detectable, especially when it is compared with APDs in all mapping sites in the M-cell layer and in the surrounding subendocardium, instead of between small numbers of microelectrode recordings. Alternatively, M cells were also defined as nonepicardial and nonendocardial cells with the longest (10th percentile) APDs.[7] This definition is difficult to interpret, because top 10% APDs can always be found even in cases with no statistically significant difference.

In the present study, we proposed a new definition, which is based on the local APD gradient between the islands of delayed repolarization (M-cells) and the neighboring myocardium (Fig. 4). When studied in isolation, cells could be compared based on their AP morphologies, resting potential and amplitude values. However, being incorporated in the connected myocardium, both their repolarization and restitution properties are dependent on both intrinsic cellular properties (i.e. time-dependent ionic currents that govern cellular repolarization) and also extrinsic factors such as propagation[32] and cell-to-cell coupling.[34, 35] Thus, repolarization of a cardiac cell incorporated into the well-coupled myocardium is significantly determined by transmembrane voltage gradients from neighboring cells that either increase or decrease APD.[36] Based on our definition, which takes into accounts both intrinsic cellular properties and extrinsic electrotonic coupling, we found the evidence of the isolated islands of delayed repolarization (M-cells) in three out of five non-failing human hearts and no evidence of these islands in failing hearts. Therefore, we suggest that characterization of heterogeneity of transmural gradient and M-cells by means of APD distribution along a transmural line may be inappropriate and requires 2D mapping. Moreover, this characterization could lead to the contradictions observed between in vivo and in vitro studies.[19]

Relationship between Cx43 and repolarization

It is presumed that normal cell-to-cell coupling through gap junction would attenuate heterogeneities between different transmural layers in syncytial preparations.[15, 35–37] The resulting current flow between neighboring cells with different intrinsic repolarization time will tend to delay recovery in cells with an intrinsically short APD and will delay recovery in cells with intrinsically short APD).[35, 37] Therefore, it has been suggested that intercellular coupling through gap junctions is an important mechanism responsible for maintaining electrophysiological heterogeneities between transmural muscle layers. Experimental evidence supports this hypothesis. Thus, it has been shown in the canine LV that subepicardial expression of Cx43, the principal gap junction protein found in ventricular myocardium, is reduced compared to midmyocardial and subendocardial layers.[6] Moreover, this Cx43 downregulation is well correlated with shorter APD at the subepicardium. Our results in the human heart revealed the same transmural pattern on Cx43 expression through the LV wall as reported by Poelzing et al[6] in the canine.

HF remodeling was reported to be associated with significant reduction of Cx43 expression. Such cellular uncoupling has been observed in animal models of HF.[15] We have expected to observe similar changes in the human heart. Accordingly, in present study, we found a significant decrease of relative transmural expression of Cx43 in failing hearts (Fig. 8), especially in the subepicardium. One would expect that cellular uncoupling caused by HF induced Cx43 downregulation may unmask the intrinsic differences in APD and reveal the distinct subpopulations of cells, which can be referred to the M-cells.[15] However, in contrast to animal models, we found that in humans HF resulted in reduction of local (Fig. 4D) and global (Fig. 3D) transmural APD gradients. It appears that the observed reduction in cell-to-

cell coupling does not correlate with concomitant decrease in dispersion of repolarization, as compared to normal well-coupled myocardium. Thus, alternative mechanisms have to be considered, such as transmural heterogeneities of ion channel expression.[8] Our future studies will focus on this hypothesis.

Limitations

There are several limitations in our study. Firstly, the study was conducted in end-stage failing and non-failing human hearts, which were considered control. However, these "control" hearts were not from entirely healthy donors (see Online Table 2) and two of them had early stage hypertrophy and coronary disease. Thus, we cannot fully extend these findings to healthy human hearts. However, all non-failing hearts were characterized as hearts without history of HF in anamnesis. Cardiac resuscitation therapy could also affect donors' heart electrophysiology. The non-failing heart #5 was obtained from the patient who died from the overdose of Tylenol which could affect on the cardiac electrophysiology and induced more distinguished islands of M-cell in this heart (Figs. 3, 5–7). Nevertheless, we did not observe any significant deviations in non-failing heart groups. Therefore, it seems possible to compare failing hearts with nonfailing donor's hearts as two separate groups with different etiology.

Secondly, during the current study, we had a limited number of human heart preparations. Only five hearts with heterogeneous disease etiologies were tested in each group. More human hearts have to be tested based on their type of cardiomyopathy. The presented results should be very carefully used when extrapolated on the other types of cardiac disease.

Thirdly, only the posterior-lateral LV ventricular wall was sampled. It is possible that other regions had different repolarization heterogeneity and provided additional islands of delayed repolarization. Our data demonstrate that multiple islands are presented in the non-failing wedge preparations. However, all in vitro studies are time-limited, and characterization of multiple tissue samples from the same heart is impossible to achieve with limited resources.

Finally, we used isolated wedge preparation and optical mapping, which have their limitations well recognized in similar animal heart preparations, i.e. local heterogeneities of APD could be a consequence of surgery and/or unavoidably altered perfusion pattern at the cut surface. As any coronary perfused transmurally dissected wedge, our preparations could contain damaged regions of myocardium due to laceration of blood vessels. This may result in a moderate degree of regional ischemia, which could affect the presented APD distribution. In the initial experiments, we have excluded five hearts form the study, which had clear evidence of ischemia in the field of view. After gaining more experience with the wedge preparations, we have not observed ischemia. Moreover, presence of consistent statistically significant transmural APD gradient at various heart rates in non-failing hearts indicates that it is likely to be a valid fining.

Summary

In conclusion, we present for the first time the transmural gradient of APD and Cx43 expression in both non-failing and failing human LV. Our results demonstrate experimental evidence of sub-endocardial population of cells with prolonged APD, as well as a transmural APD gradient in the non-failing human heart. HF results in the heterogeneous prolongation of APD and thus flattens the steepness of the transmural APD gradient.

Supplementary Material

Refer to Web version on PubMed Central for supplementary material.

Acknowledgments

The authors thank Stefanie J. Tanenhaus and Ai-Li Cai for tissue preparation and technical support.

Sources of funding

This work was supported by NIH R01 grants HL085369, HL067322, and HL074283.

Non-standard Abbreviations and Acronyms

HF	heart failure
EP	electrophysiology
M-cells	midmyocardial cells with prolonged repolarization
LV	left ventricle
CL	cycle length
AP	action potential
APD	action potential duration
DI	diastolic interval
Max-APD	action potential duration in the islands with prolonged repolarization

References

1. Jin H, Lyon AR, Akar FG. Arrhythmia mechanisms in the failing heart. Pacing Clin Electrophysiol 2008;31:1048–1056. [PubMed: 18684263]
2. Tomaselli GF, Zipes DP. What causes sudden death in heart failure? Circ Res 2004;95:754–763. [PubMed: 15486322]
3. Nass RD, Aiba T, Tomaselli GF, Akar FG. Mechanisms of disease: ion channel remodeling in the failing ventricle. Nat Clin Pract Cardiovasc Med 2008;5:196–207. [PubMed: 18317475]
4. Akar FG, Rosenbaum DS. Transmural electrophysiological heterogeneities underlying arrhythmogenesis in heart failure. Circ Res 2003;93:638–645. [PubMed: 12933704]
5. Tomaselli GF, Marban E. Electrophysiological remodeling in hypertrophy and heart failure. Cardiovasc Res 1999;42:270–283. [PubMed: 10533566]
6. Poelzing S, Akar FG, Baron E, Rosenbaum DS. Heterogeneous connexin43 expression produces electrophysiological heterogeneities across ventricular wall. Am J Physiol Heart Circ Physiol 2004;286:H2001–2009. [PubMed: 14704225]
7. Akar FG, Yan GX, Antzelevitch C, Rosenbaum DS. Unique topographical distribution of M cells underlies reentrant mechanism of torsade de pointes in the long-QT syndrome. Circulation 2002;105:1247–1253. [PubMed: 11889021]
8. Antzelevitch C. Role of spatial dispersion of repolarization in inherited and acquired sudden cardiac death syndromes. Am J Physiol Heart Circ Physiol 2007;293:H2024–2038. [PubMed: 17586620]
9. Anyukhovsky EP, Sosunov EA, Rosen MR. Regional differences in electrophysiological properties of epicardium, midmyocardium, and endocardium. In vitro and in vivo correlations. Circulation 1996;94:1981–1988. [PubMed: 8873677]
10. Sosunov EA, Anyukhovsky EP, Rosen MR. Effects of quinidine on repolarization in canine epicardium, midmyocardium, and endocardium: I. In vitro study. Circulation 1997;96:4011–4018. [PubMed: 9403626]
11. Antzelevitch C, Sicouri S, Litovsky SH, Lukas A, Krishnan SC, Di Diego JM, Gintant GA, Liu DW. Heterogeneity within the ventricular wall. Electrophysiology and pharmacology of epicardial, endocardial, and M cells. Circ Res 1991;69:1427–1449. [PubMed: 1659499]
12. Weissenburger J, Nesterenko VV, Antzelevitch C. Transmural heterogeneity of ventricular repolarization under baseline and long QT conditions in the canine heart in vivo: torsades de pointes

develops with halothane but not pentobarbital anesthesia. J Cardiovasc Electrophysiol 2000;11:290–304. [PubMed: 10749352]

13. Drouin E, Charpentier F, Gauthier C, Laurent K, Le Marec H. Electrophysiologic characteristics of cells spanning the left ventricular wall of human heart: evidence for presence of M cells. J Am Coll Cardiol 1995;26:185–192. [PubMed: 7797750]
14. Chauhan VS, Downar E, Nanthakumar K, Parker JD, Ross HJ, Chan W, Picton P. Increased ventricular repolarization heterogeneity in patients with ventricular arrhythmia vulnerability and cardiomyopathy: a human in vivo study. Am J Physiol Heart Circ Physiol 2006;290:H79–86. [PubMed: 16113076]
15. Poelzing S, Rosenbaum DS. Altered connexin43 expression produces arrhythmia substrate in heart failure. Am J Physiol Heart Circ Physiol 2004;287:H1762–1770. [PubMed: 15205174]
16. Taggart P, Sutton PM, Opthof T, Coronel R, Trimlett R, Pugsley W, Kallis P. Transmural repolarisation in the left ventricle in humans during normoxia and ischaemia. Cardiovasc Res 2001;50:454–462. [PubMed: 11376621]
17. Ueda N, Zipes DP, Wu J. Functional and transmural modulation of M cell behavior in canine ventricular wall. Am J Physiol Heart Circ Physiol 2004;287:H2569–2575. [PubMed: 15331367]
18. Voss F, Opthof T, Marker J, Bauer A, Katus HA, Becker R. There is no transmural heterogeneity in an index of action potential duration in the canine left ventricle. Heart Rhythm 2009;6:1028–1034. [PubMed: 19560091]
19. Anyukhovsky EP, Sosunov EA, Gainullin RZ, Rosen MR. The controversial M cell. J Cardiovasc Electrophysiol 1999;10:244–260. [PubMed: 10090229]
20. Antzelevitch C, Shimizu W, Yan GX, Sicouri S, Weissenburger J, Nesterenko VV, Burashnikov A, Di Diego J, Saffitz J, Thomas GP. The M cell: its contribution to the ECG and to normal and abnormal electrical function of the heart. J Cardiovasc Electrophysiol 1999;10:1124–1152. [PubMed: 10466495]
21. Dou Y, Arlock P, Arner A. Blebbistatin specifically inhibits actin-myosin interaction in mouse cardiac muscle. Am J Physiol Cell Physiol 2007;293:C1148–1153. [PubMed: 17615158]
22. Fedorov VV, Lozinsky IT, Sosunov EA, Anyukhovsky EP, Rosen MR, Balke CW, Efimov IR. Application of blebbistatin as an excitation-contraction uncoupler for electrophysiologic study of rat and rabbit hearts. Heart Rhythm 2007;4:619–626. [PubMed: 17467631]
23. Glukhov AV, Flagg TP, Fedorov VV, Efimov IR, Nichols CG. Differential K(ATP) channel pharmacology in intact mouse heart. J Mol Cell Cardiol. 2009
24. Fedorov VV, Kostecki G, Hemphill M, Efimov IR. Atria are more susceptible to electroporation than ventricles: implications for atrial stunning, shock-induced arrhythmia and defibrillation failure. Heart Rhythm 2008;5:593–604. [PubMed: 18362029]
25. Fedorov VV, Glukhov AV, Sudharshan S, Egorov Y, Rosenshtraukh LV, Efimov IR. Electrophysiological mechanisms of antiarrhythmic protection during hypothermia in winter hibernating versus nonhibernating mammals. Heart Rhythm 2008;5:1587–1596. [PubMed: 18984537]
26. Narayan SM, Franz MR, Lalani G, Kim J, Sastry A. T-wave alternans, restitution of human action potential duration, and outcome. J Am Coll Cardiol 2007;50:2385–2392. [PubMed: 18154963]
27. Fedorov VV, Schuessler RB, Hemphill M, Ambrosi CM, Chang R, Voloshina AS, Brown K, Hucker WJ, Efimov IR. Structural and functional evidence for discrete exit pathways that connect the canine sinoatrial node and atria. Circ Res 2009;104:915–923. [PubMed: 19246679]
28. Hucker WJ, McCain ML, Laughner JI, Iaizzo PA, Efimov IR. Connexin 43 expression delineates two discrete pathways in the human atrioventricular junction. Anat Rec (Hoboken) 2008;291:204–215. [PubMed: 18085635]
29. Durrer D, van Dam RT, Freud GE, Janse MJ, Meijler FL, Arzbaecher RC. Total excitation of the isolated human heart. Circulation 1970;41:899–912. [PubMed: 5482907]
30. Sicouri S, Antzelevitch C. A subpopulation of cells with unique electrophysiological properties in the deep subepicardium of the canine ventricle. The M cell. Circ Res 1991;68:1729–1741. [PubMed: 2036721]
31. Efimov IR, Huang DT, Rendt JM, Salama G. Optical mapping of repolarization and refractoriness from intact hearts. Circulation 1994;90:1469–1480. [PubMed: 8087954]

32. Gotoh M, Uchida T, Fan W, Fishbein MC, Karagueuzian HS, Chen PS. Anisotropic repolarization in ventricular tissue. Am J Physiol 1997;272:H107–113. [PubMed: 9038928]

33. Yan GX, Shimizu W, Antzelevitch C. Characteristics and distribution of M cells in arterially perfused canine left ventricular wedge preparations. Circulation 1998;98:1921–1927. [PubMed: 9799214]

34. Lesh MD, Pring M, Spear JF. Cellular uncoupling can unmask dispersion of action potential duration in ventricular myocardium. A computer modeling study. Circ Res 1989;65:1426–1440. [PubMed: 2805251]

35. Conrath CE, Wilders R, Coronel R, de Bakker JM, Taggart P, de Groot JR, Opthof T. Intercellular coupling through gap junctions masks M cells in the human heart. Cardiovasc Res 2004;62:407–414. [PubMed: 15094360]

36. Laurita KR, Girouard SD, Rudy Y, Rosenbaum DS. Role of passive electrical properties during action potential restitution in intact heart. Am J Physiol 1997;273:H1205–1214. [PubMed: 9321808]

37. Viswanathan PC, Shaw RM, Rudy Y. Effects of IKr and IKs heterogeneity on action potential duration and its rate dependence: a simulation study. Circulation 1999;99:2466–2474. [PubMed: 10318671]

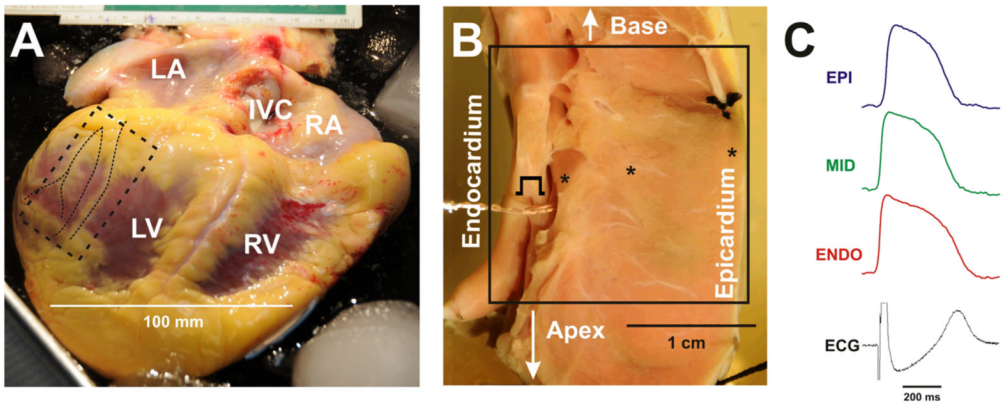

Figure 1. Human left ventricular wedge preparation

The hearts with cardiomyopathy were available during transplantation (**A**). For control, non-failing hearts, which were rejected for transplantation, were used. The action potentials were optically mapped in the coronary-perfused and superfused LV wedge preparations (**B,** non-failing heart #3). Tissue samples from the posterior-lateral LV free wall were used. The sample began several centimeters below the base of the ventricles and extends about 3 cm towards the apex (marked by dotted rectangle on **A**). The sample was cannulated through the main coronary artery supplying the surrounding tissue. Other small arteries were ligated and an adequate perfusion pressure was maintained (shown on **B**). The optical field of view is denoted by square on photo **B**. The examples of optical action potential recordings (at pacing CL=2,000 ms) from the subepicardium, midmyocardium, and subendocardium as well as ECG are presented in **C**.

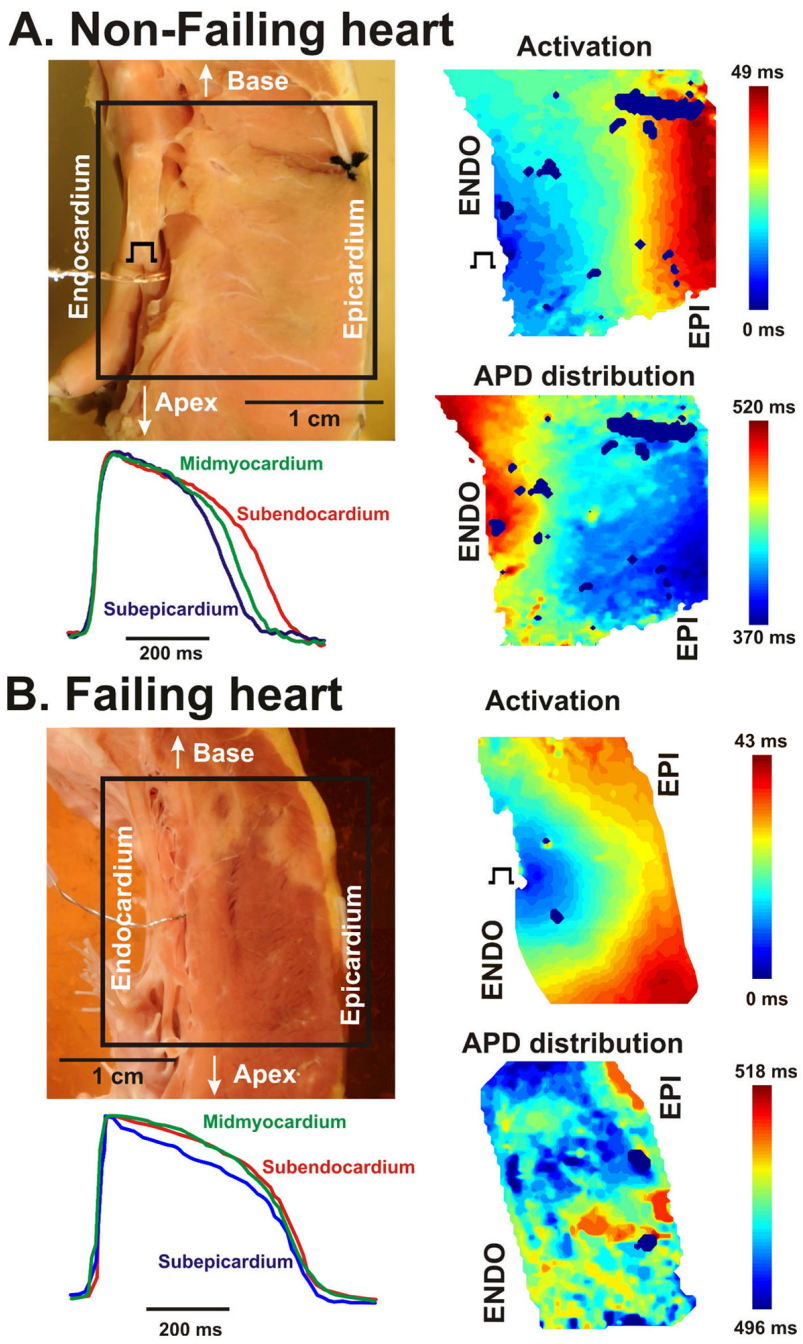

Figure 2. Optical mapping of LV wedge preparation

Transmural activation and APD distribution contour maps from non-failing (A, heart #3) and failing (B, heart #4) human hearts are shown at pacing CL=2,000 ms. Optical fields of view are denoted by rectangles on corresponding photos. Endocardial pacing sites are marked. Color scales represent the activation time and APD in corresponding maps. Selected subepicardial (EPI), midmyocardial (MID), and subendocardial (ENDO) action potentials are superimposed and demonstrated for each heart.

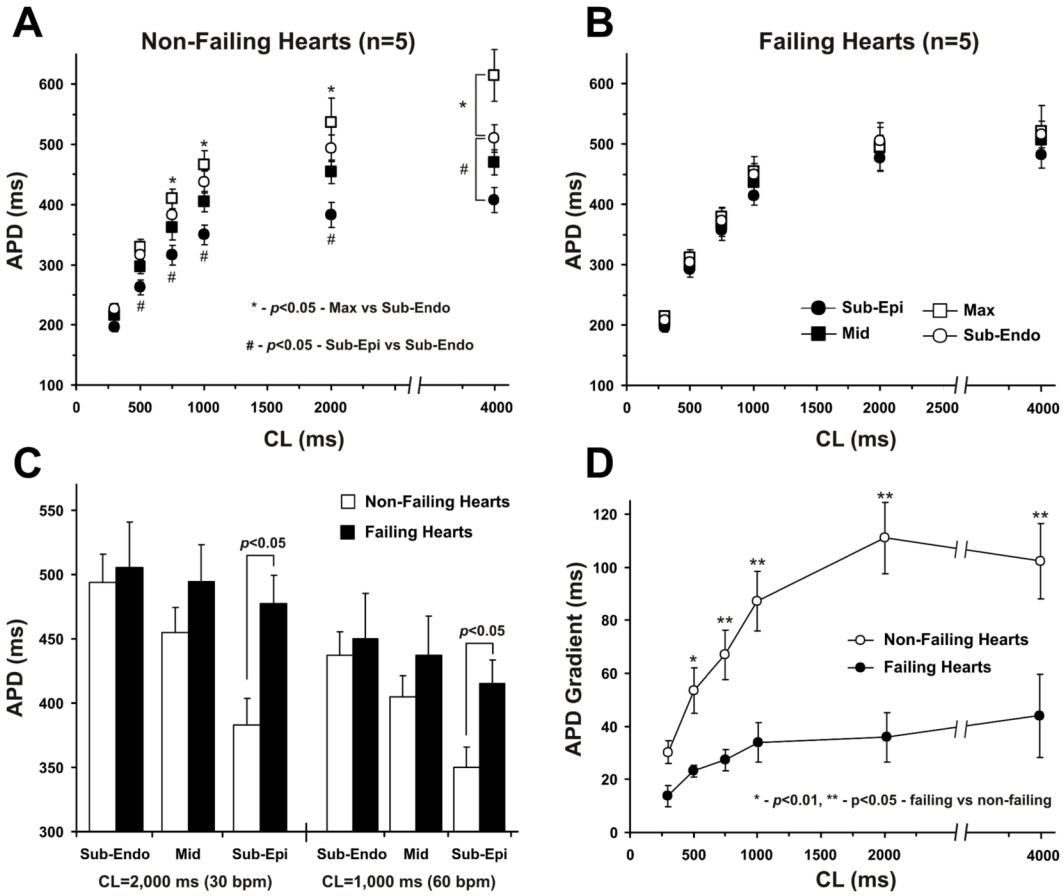

Figure 3. Summary data for transmural distribution of action potential duration (APD) in non-failing (n=5) and failing (n=5) human hearts

A. Transmural APD80 distribution in non-failing human hearts at different pacing CL. APD80 were calculated for different transmural areas: sub-epicardium, midmyocardium, sub-endocardium and in the region with the longest APDs (Max). * - $p<0.05$ for Max cells versus subendocardium; # - $p<0.05$ for subepicardium versus subendocardium.

B. Transmural APD distribution in failing human hearts at different pacing CL.

C. APD80 for subendocardial (Sub-Endo), midmyocardial (Mid), and subepicardial (Sub-Epi) layers are presented for non-failing and failing human hearts at 2,000 ms and 1,000 ms pacing CL. * - $p<0.05$ for non-failing versus failing groups.

D. Transmural APD gradients calculated as a difference between the subepicardial and subendocardial APD80 throughout the mapped area are presented for non-failing and failing hearts at different pacing CL. * - $p<0.01$, ** - $p<0.05$ for non-failing versus failing groups.

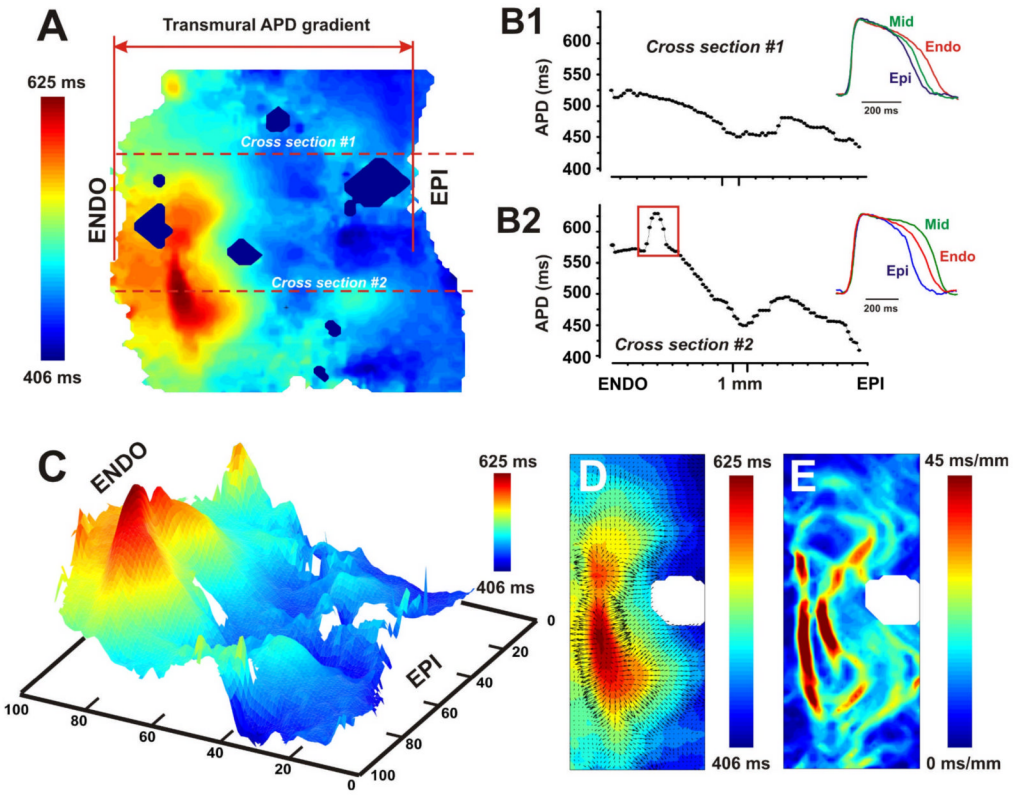

Figure 4. Local action potential duration (APD) gradient as a criterion for definition of islands of cells with prolonged repolarization

The example of the transmural APD distribution contour map is shown (**A**). Data from the non-failing heart #5 at pacing CL=2,000 ms was used. Two types of APD distribution through the LV wall are plotted for two cross sections (red horizontal dotted lines) passed beyond (**B1**) and over (**B2**) the island of prolonged repolarization (trough the cross sections #1 and #2, respectively) marked by the black dotted curve. Selected from the cross section, subepicardial (EPI), midmyocardial (MID), and subendocardial (ENDO) action potentials are superimposed and presented for each APD distribution in **B1** and **B2**. The spatial resolution for this wedge was about 190 μm per pixel. Red rectangle on the **panel B2** selects the area of cells with prolonged repolarization in the deep subendocardium. **Panel C** represents a pseudo-3D map of APD distribution shown in **A**. Max-APD island is shown in red and characterized be the sharp local APD gradient around it. **Panel D** demonstrates the magnitude and direction of local APD gradient vectors. The representative example of distribution of the local APD gradient calculated throughout the mapped area is shown in **panel E**.

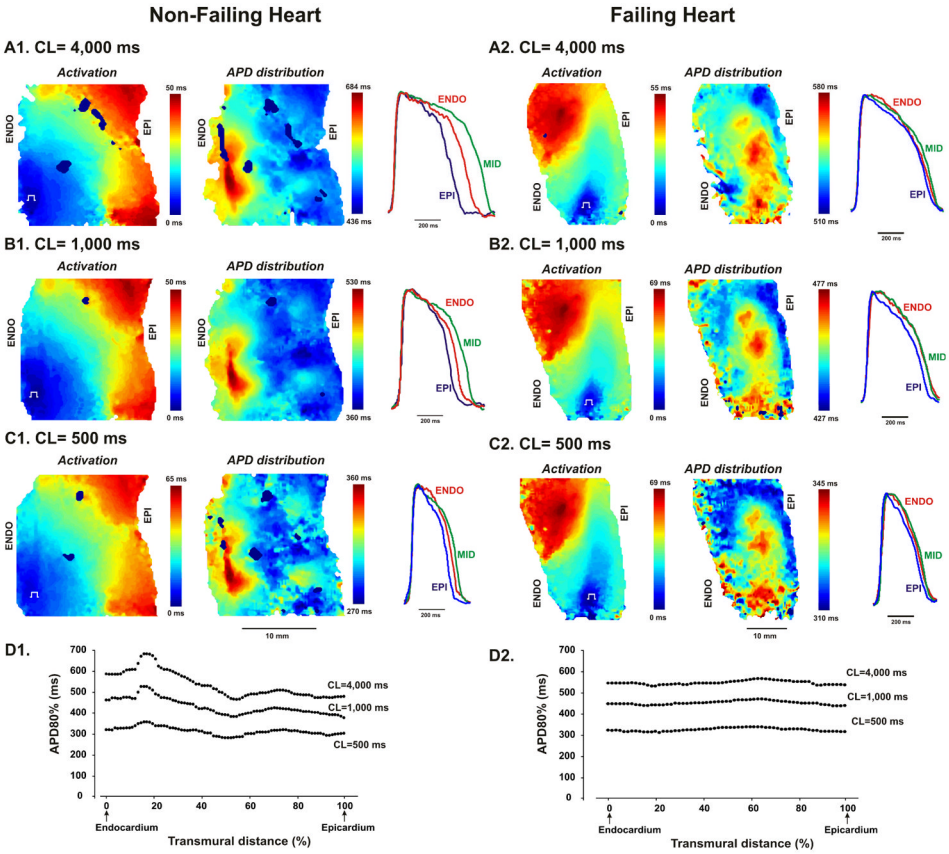

Figure 5. Examples of activation and action potential (APD) distribution patterns for non-failing and failing human wedge preparations obtained at different pacing CL during restitution measurements

Data are presented for the non-failing heart #5 and failing heart #2. Three pacing CLs (4,000ms, 1,000ms, and 500ms) from the applied restitution protocol are shown. Superimposed action potentials from the epicardial (EPI), midmyocardial (MID), and endocardial (ENDO) layers are presented for each pacing CL. On the bottom panels, transmural APD distributions at different pacing CL are presented for non-failing (**D1**) and failing (**D2**) hearts.

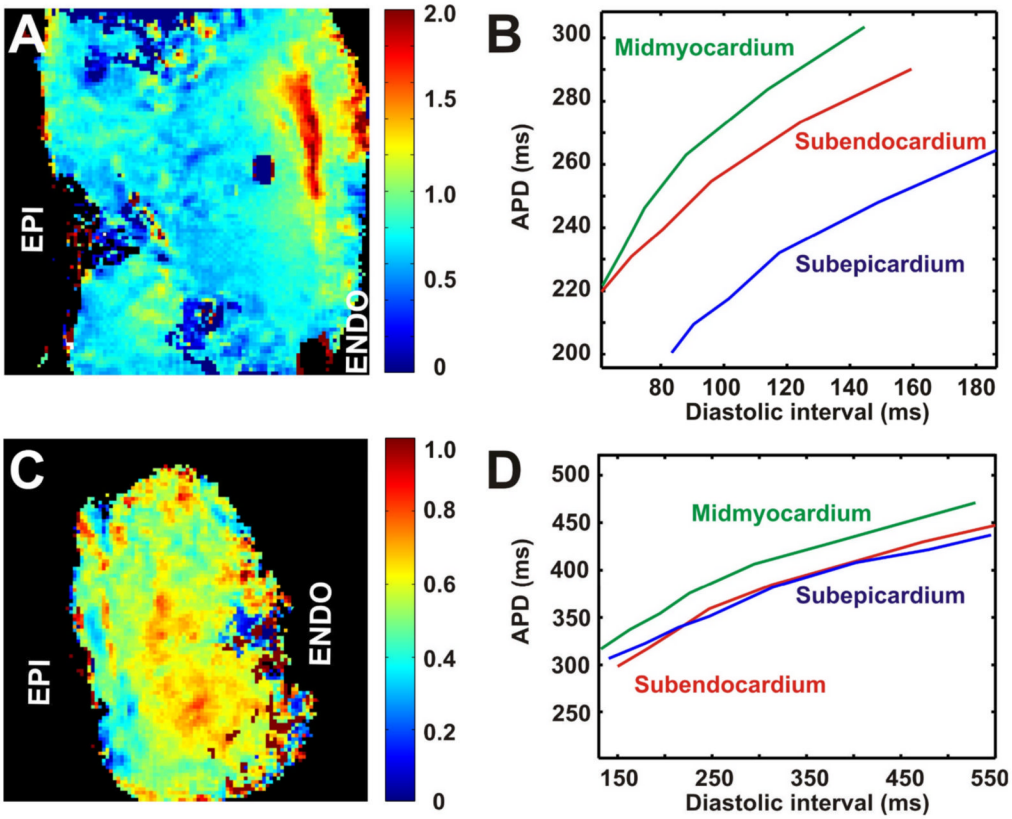

Figure 6. Spatial distribution of action potential duration (APD) restitution through the LV free wall

Data are presented for the non-failing heart #5 (**A**) and failing heart #2 (**B**). Spatial distributions of slopes for APD restitution curve for each pixel through the mapped area are presented on the right panels. On the left panels, three restitution curves plotted for pixels from subepicardium, midmyocardium and subendocardium are shown.

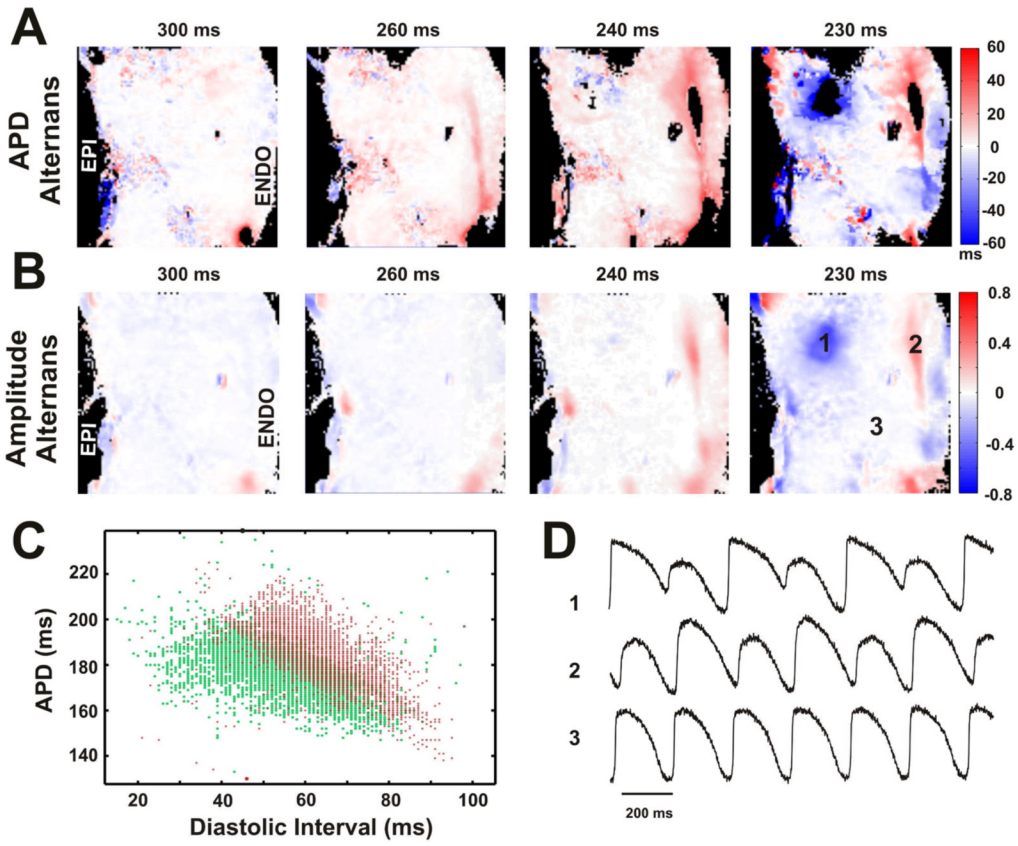

Figure 7. Dynamics and localization of action potential duration (A) and action potential amplitude (B) alternans

Data are presented for the non-failing heart #5. Four panels in (**A**) and (**B**) represent transmural distribution of alternans during progressive decrease of pacing CL. Colors indicate the amplitude of alternans which can be positive (red) or negative (blue) relative to no alternans (white). **C:** Plot of APDs against diastolic intervals of consecutive two beats (represented by red and green respectively) for each pixel during pacing with CL of 240ms. The separation of areas with single colors (red or green) indicates the presence of alternans. **D:** The representative examples of optical recordings from three areas labeled on maps.

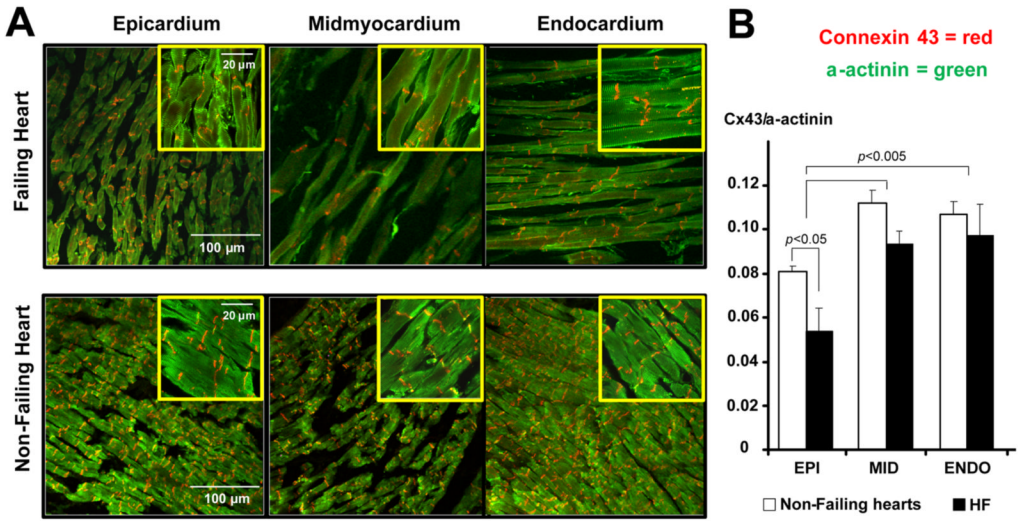

Figure 8. Transmural expression of connexin 43

A: Sample confocal images from non-failing and failing hearts taken from the subepicardium, midmyocardium, and subendocardium using a 20x magnification. For each image, the zoomed areas with 100x magnification are presented in corresponding insets. The expression of Cx43 is presented in red, α-actinin – in green. **B:** Average Cx43 densities at each tissue location. We analyzed 5 randomly selected fields of view in each area of myocardium obtained at 20x magnification. For each image, the ratio of Cx43 to α-actinin was calculated. Average data represent non-failing (n=4) and failing (HF, n=3) human hearts.